EUROPEAN ORGANIZATION FOR NUCLEAR RESEARCH

CERN–EP-2000-051

7 April 2000

A search for invisible Higgs bosons produced in e^+e^- interactions up to $\sqrt{s} = 189$ GeV

DELPHI Collaboration

Abstract

Searches for HZ production with the Higgs boson decaying into an invisible final state have been performed with the data collected by the DELPHI experiment up to the centre-of-mass energy of 188.6 GeV. The hadronic and muon pair final states of the Z boson were analysed. No signal was found. Upper limits on the cross-section and the corresponding Higgs boson mass limits were set at 95% confidence level. Combining these results with DELPHI results for the visible modes, a 95% confidence level Higgs mass lower limit of 92.3 GeV was obtained, independent of the branching ratio into visible and invisible decays.

P.Abreu[22], W.Adam[52], T.Adye[38], P.Adzic[12], Z.Albrecht[18], T.Alderweireld[2], G.D.Alekseev[17], R.Alemany[51], T.Allmendinger[18], P.P.Allport[23], S.Almehed[25], U.Amaldi[29], N.Amapane[47], S.Amato[49], E.G.Anassontzis[3], P.Andersson[46], A.Andreazza[28], S.Andringa[22], P.Antilogus[26], W-D.Apel[18], Y.Arnoud[15], B.Åsman[46], J-E.Augustin[24], A.Augustinus[9], P.Baillon[9], A.Ballestrero[47], P.Bambade[9,20], F.Barao[22], G.Barbiellini[48], R.Barbier[26], D.Y.Bardin[17], G.Barker[18], A.Baroncelli[40], M.Battaglia[16], M.Baubillier[24], K-H.Becks[54], M.Begalli[6], A.Behrmann[54], P.Beilliere[8], Yu.Belokopytov[9], K.Belous[44], N.C.Benekos[33], A.C.Benvenuti[5], C.Berat[15], M.Berggren[24], L.Berntzon[46], D.Bertrand[2], M.Besancon[41], M.S.Bilenky[17], M-A.Bizouard[20], D.Bloch[10], H.M.Blom[32], M.Bonesini[29], M.Boonekamp[41], P.S.L.Booth[23], G.Borisov[20], C.Bosio[43], O.Botner[50], E.Boudinov[32], B.Bouquet[20], C.Bourdarios[20], T.J.V.Bowcock[23], I.Boyko[17], I.Bozovic[12], M.Bozzo[14], M.Bracko[45], P.Branchini[40], R.A.Brenner[50], P.Bruckman[9], J-M.Brunet[8], L.Bugge[34], T.Buran[34], B.Buschbeck[52], P.Buschmann[54], S.Cabrera[51], M.Caccia[28], M.Calvi[29], T.Camporesi[9], V.Canale[39], F.Carena[9], L.Carroll[23], C.Caso[14], M.V.Castillo Gimenez[51], A.Cattai[9], F.R.Cavallo[5], M.Chapkin[44], Ph.Charpentier[9], P.Checchia[37], G.A.Chelkov[17], R.Chierici[47], P.Chliapnikov[9,44], P.Chochula[7], V.Chorowicz[26], J.Chudoba[31], K.Cieslik[19], P.Collins[9], R.Contri[14], E.Cortina[51], G.Cosme[20], F.Cossutti[9], M.Costa[51], H.B.Crawley[1], D.Crennell[38], G.Crosetti[14], J.Cuevas Maestro[35], S.Czellar[16], J.D'Hondt[2], J.Dalmau[46], M.Davenport[9], W.Da Silva[24], G.Della Ricca[48], P.Delpierre[27], N.Demaria[47], A.De Angelis[48], W.De Boer[18], C.De Clercq[2], B.De Lotto[48], A.De Min[9], L.De Paula[49], H.Dijkstra[9], L.Di Ciaccio[39], J.Dolbeau[8], K.Doroba[53], M.Dracos[10], J.Drees[54], M.Dris[33], G.Eigen[4], T.Ekelof[50], M.Ellert[50], M.Elsing[9], J-P.Engel[10], M.Espirito Santo[9], G.Fanourakis[12], D.Fassouliotis[12], M.Feindt[18], J.Fernandez[42], A.Ferrer[51], E.Ferrer-Ribas[20], F.Ferro[14], A.Firestone[1], U.Flagmeyer[54], H.Foeth[9], E.Fokitis[33], F.Fontanelli[14], B.Franek[38], A.G.Frodesen[4], R.Fruhwirth[52], F.Fulda-Quenzer[20], J.Fuster[51], A.Galloni[23], D.Gamba[47], S.Gamblin[20], M.Gandelman[49], C.Garcia[51], C.Gaspar[9], M.Gaspar[49], U.Gasparini[37], Ph.Gavillet[9], E.N.Gazis[33], D.Gele[10], T.Geralis[12], N.Ghodbane[26], I.Gil[51], F.Glege[54], R.Gokieli[9,53], B.Golob[9,45], G.Gomez-Ceballos[42], P.Goncalves[22], I.Gonzalez Caballero[42], G.Gopal[38], L.Gorn[1], Yu.Gouz[44], V.Gracco[14], J.Grahl[1], E.Graziani[40], P.Gris[41], G.Grosdidier[20], K.Grzelak[53], J.Guy[38], C.Haag[18], F.Hahn[9], S.Hahn[54], S.Haider[9], A.Hallgren[50], K.Hamacher[54], J.Hansen[34], F.J.Harris[36], F.Hauler[18], V.Hedberg[9,25], S.Heising[18], J.J.Hernandez[51], P.Herquet[2], H.Herr[9], E.Higon[51], S-O.Holmgren[46], P.J.Holt[36], S.Hoorelbeke[2], M.Houlden[23], J.Hrubec[52], M.Huber[18], G.J.Hughes[23], K.Hultqvist[9,46], J.N.Jackson[23], R.Jacobsson[9], P.Jalocha[19], R.Janik[7], Ch.Jarlskog[25], G.Jarlskog[25], P.Jarry[41], B.Jean-Marie[20], D.Jeans[36], E.K.Johansson[46], P.Jonsson[26], C.Joram[9], P.Juillot[10], L.Jungermann[18], F.Kapusta[24], K.Karafasoulis[12], S.Katsanevas[26], E.C.Katsoufis[33], R.Keranen[18], G.Kernel[45], B.P.Kersevan[45], Yu.Khokhlov[44], B.A.Khomenko[17], N.N.Khovanski[17], A.Kiiskinen[16], B.King[23], A.Kinvig[23], N.J.Kjaer[9], O.Klapp[54], P.Kluit[32], P.Kokkinias[12], V.Kostioukhine[44], C.Kourkoumelis[3], O.Kouznetsov[17], M.Krammer[52], E.Kriznic[45], Z.Krumstein[17], P.Kubinec[7], J.Kurowska[53], K.Kurvinen[16], J.W.Lamsa[1], D.W.Lane[1], V.Lapin[44], J-P.Laugier[41], R.Lauhakangas[16], G.Leder[52], F.Ledroit[15], L.Leinonen[46], A.Leisos[12], R.Leitner[31], G.Lenzen[54], V.Lepeltier[20], T.Lesiak[19], M.Lethuillier[26], J.Libby[36], W.Liebig[54], D.Liko[9], A.Lipniacka[46], I.Lippi[37], B.Loerstad[25], J.G.Loken[36], J.H.Lopes[49], J.M.Lopez[42], R.Lopez-Fernandez[15], D.Loukas[12], P.Lutz[41], L.Lyons[36], J.MacNaughton[52], J.R.Mahon[6], A.Maio[22], A.Malek[54], S.Maltezos[33], V.Malychev[17], F.Mandl[52], J.Marco[42], R.Marco[42], B.Marechal[49], M.Margoni[37], J-C.Marin[9], C.Mariotti[9], A.Markou[12], C.Martinez-Rivero[9], S.Marti i Garcia[9], J.Masik[13], N.Mastroyiannopoulos[12], F.Matorras[42], C.Matteuzzi[29], G.Matthiae[39], F.Mazzucato[37], M.Mazzucato[37], M.Mc Cubbin[23], R.Mc Kay[1], R.Mc Nulty[23], G.Mc Pherson[23], E.Merle[15], C.Meroni[28], W.T.Meyer[1], A.Miagkov[44], E.Migliore[9], L.Mirabito[26], W.A.Mitaroff[52], U.Mjoernmark[25], T.Moa[46], M.Moch[18], R.Moeller[30], K.Moenig[9,11], M.R.Monge[14], D.Moraes[49], P.Morettini[14], G.Morton[36], U.Mueller[54], K.Muenich[54], M.Mulders[32], C.Mulet-Marquis[15], L.M.Mundim[6], R.Muresan[25], W.J.Murray[38], B.Muryn[19], G.Myatt[36], T.Myklebust[34], F.Naraghi[15], M.Nassiakou[12], F.L.Navarria[5], K.Nawrocki[53], P.Negri[29], N.Neufeld[52], R.Nicolaidou[41], B.S.Nielsen[30], P.Niezurawski[53], M.Nikolenko[10,17], V.Nomokonov[16], A.Nygren[25], V.Obraztsov[44], A.G.Olshevski[17], A.Onofre[22], R.Orava[16], G.Orazi[10], K.Osterberg[9], A.Ouraou[41], A.Oyanguren[51], M.Paganoni[29], S.Paiano[5], R.Pain[24], R.Paiva[22], J.Palacios[36], H.Palka[19], Th.D.Papadopoulou[33], L.Pape[9], C.Parkes[9], F.Parodi[14], U.Parzefall[23], A.Passeri[40], O.Passon[54], T.Pavel[25], M.Pegoraro[37], L.Peralta[22], M.Pernicka[52], A.Perrotta[5], C.Petridou[48], A.Petrolini[14], H.T.Phillips[38], F.Pierre[41], M.Pimenta[22], E.Piotto[28], T.Podobnik[45], V.Poireau[41], M.E.Pol[6], G.Polok[19], P.Poropat[48], V.Pozdniakov[17], P.Privitera[39], N.Pukhaeva[17], A.Pullia[29], D.Radojicic[36], S.Ragazzi[29], H.Rahmani[33], J.Rames[13], P.N.Ratoff[21], A.L.Read[34], P.Rebecchi[9], N.G.Redaelli[29], M.Regler[52], J.Rehn[18], D.Reid[32], P.Reinertsen[4], R.Reinhardt[54], P.B.Renton[36], L.K.Resvanis[3], F.Richard[20], J.Ridky[13], G.Rinaudo[47], I.Ripp-Baudot[10], A.Romero[47], P.Ronchese[37], E.I.Rosenberg[1], P.Rosinsky[7], P.Roudeau[20], T.Rovelli[5], V.Ruhlmann-Kleider[41], A.Ruiz[42], H.Saarikko[16], Y.Sacquin[41], A.Sadovsky[17], G.Sajot[15], J.Salt[51], D.Sampsonidis[12], M.Sannino[14], A.Savoy-Navarro[24], Ph.Schwemling[24], B.Schwering[54], U.Schwickerath[18], F.Scuri[48], P.Seager[21], Y.Sedykh[17], A.M.Segar[36], N.Seibert[18], R.Sekulin[38], G.Sette[14], R.C.Shellard[6], M.Siebel[54], L.Simard[41], F.Simonetto[37], A.N.Sisakian[17], G.Smadja[26], O.Smirnova[25], G.R.Smith[38], O.Solovianov[44], A.Sopczak[18], R.Sosnowski[53], T.Spassov[9], E.Spiriti[40], S.Squarcia[14], C.Stanescu[40], M.Stanitzki[18], K.Stevenson[36], A.Stocchi[20], J.Strauss[52], R.Strub[10], B.Stugu[4], M.Szczekowski[53], M.Szeptycka[53], T.Tabarelli[29], A.Taffard[23], F.Tegenfeldt[50], F.Terranova[29], J.Timmermans[32], N.Tinti[5], L.G.Tkatchev[17], M.Tobin[23], S.Todorova[9], B.Tome[22], A.Tonazzo[9], L.Tortora[40], P.Tortosa[51], G.Transtromer[25], D.Treille[9], G.Tristram[8], M.Trochimczuk[53], C.Troncon[28], M-L.Turluer[41], I.A.Tyapkin[17], P.Tyapkin[25], S.Tzamarias[12], O.Ullaland[9], V.Uvarov[44], G.Valenti[9,5], E.Vallazza[48], P.Van Dam[32], W.Van den Boeck[2], W.K.Van Doninck[2], J.Van Eldik[9,32], A.Van Lysebetten[2],

N.van Remortel[2], I.Van Vulpen[32], G.Vegni[28], L.Ventura[37], W.Venus[38,9], F.Verbeure[2], P.Verdier[26], M.Verlato[37], L.S.Vertogradov[17], V.Verzi[28], D.Vilanova[41], L.Vitale[48], E.Vlasov[44], A.S.Vodopyanov[17], G.Voulgaris[3], V.Vrba[13], H.Wahlen[54], A.J.Washbrook[23], C.Weiser[9], D.Wicke[9], J.H.Wickens[2], G.R.Wilkinson[36], M.Winter[10], M.Witek[19], G.Wolf[9], J.Yi[1], O.Yushchenko[44], A.Zalewska[19], P.Zalewski[53], D.Zavrtanik[45], E.Zevgolatakos[12], N.I.Zimin[17,25], A.Zintchenko[17], Ph.Zoller[10], G.Zumerle[37], M.Zupan[12]

[1] Department of Physics and Astronomy, Iowa State University, Ames IA 50011-3160, USA
[2] Physics Department, Univ. Instelling Antwerpen, Universiteitsplein 1, B-2610 Antwerpen, Belgium
and IIHE, ULB-VUB, Pleinlaan 2, B-1050 Brussels, Belgium
and Faculté des Sciences, Univ. de l'Etat Mons, Av. Maistriau 19, B-7000 Mons, Belgium
[3] Physics Laboratory, University of Athens, Solonos Str. 104, GR-10680 Athens, Greece
[4] Department of Physics, University of Bergen, Allégaten 55, NO-5007 Bergen, Norway
[5] Dipartimento di Fisica, Università di Bologna and INFN, Via Irnerio 46, IT-40126 Bologna, Italy
[6] Centro Brasileiro de Pesquisas Físicas, rua Xavier Sigaud 150, BR-22290 Rio de Janeiro, Brazil
and Depto. de Física, Pont. Univ. Católica, C.P. 38071 BR-22453 Rio de Janeiro, Brazil
and Inst. de Física, Univ. Estadual do Rio de Janeiro, rua São Francisco Xavier 524, Rio de Janeiro, Brazil
[7] Comenius University, Faculty of Mathematics and Physics, Mlynska Dolina, SK-84215 Bratislava, Slovakia
[8] Collège de France, Lab. de Physique Corpusculaire, IN2P3-CNRS, FR-75231 Paris Cedex 05, France
[9] CERN, CH-1211 Geneva 23, Switzerland
[10] Institut de Recherches Subatomiques, IN2P3 - CNRS/ULP - BP20, FR-67037 Strasbourg Cedex, France
[11] Now at DESY-Zeuthen, Platanenallee 6, D-15735 Zeuthen, Germany
[12] Institute of Nuclear Physics, N.C.S.R. Demokritos, P.O. Box 60228, GR-15310 Athens, Greece
[13] FZU, Inst. of Phys. of the C.A.S. High Energy Physics Division, Na Slovance 2, CZ-180 40, Praha 8, Czech Republic
[14] Dipartimento di Fisica, Università di Genova and INFN, Via Dodecaneso 33, IT-16146 Genova, Italy
[15] Institut des Sciences Nucléaires, IN2P3-CNRS, Université de Grenoble 1, FR-38026 Grenoble Cedex, France
[16] Helsinki Institute of Physics, HIP, P.O. Box 9, FI-00014 Helsinki, Finland
[17] Joint Institute for Nuclear Research, Dubna, Head Post Office, P.O. Box 79, RU-101 000 Moscow, Russian Federation
[18] Institut für Experimentelle Kernphysik, Universität Karlsruhe, Postfach 6980, DE-76128 Karlsruhe, Germany
[19] Institute of Nuclear Physics and University of Mining and Metalurgy, Ul. Kawiory 26a, PL-30055 Krakow, Poland
[20] Université de Paris-Sud, Lab. de l'Accélérateur Linéaire, IN2P3-CNRS, Bât. 200, FR-91405 Orsay Cedex, France
[21] School of Physics and Chemistry, University of Lancaster, Lancaster LA1 4YB, UK
[22] LIP, IST, FCUL - Av. Elias Garcia, 14-1°, PT-1000 Lisboa Codex, Portugal
[23] Department of Physics, University of Liverpool, P.O. Box 147, Liverpool L69 3BX, UK
[24] LPNHE, IN2P3-CNRS, Univ. Paris VI et VII, Tour 33 (RdC), 4 place Jussieu, FR-75252 Paris Cedex 05, France
[25] Department of Physics, University of Lund, Sölvegatan 14, SE-223 63 Lund, Sweden
[26] Université Claude Bernard de Lyon, IPNL, IN2P3-CNRS, FR-69622 Villeurbanne Cedex, France
[27] Univ. d'Aix - Marseille II - CPP, IN2P3-CNRS, FR-13288 Marseille Cedex 09, France
[28] Dipartimento di Fisica, Università di Milano and INFN-MILANO, Via Celoria 16, IT-20133 Milan, Italy
[29] Dipartimento di Fisica, Univ. di Milano-Bicocca and INFN-MILANO, Piazza delle Scienze 2, IT-20126 Milan, Italy
[30] Niels Bohr Institute, Blegdamsvej 17, DK-2100 Copenhagen Ø, Denmark
[31] IPNP of MFF, Charles Univ., Areal MFF, V Holesovickach 2, CZ-180 00, Praha 8, Czech Republic
[32] NIKHEF, Postbus 41882, NL-1009 DB Amsterdam, The Netherlands
[33] National Technical University, Physics Department, Zografou Campus, GR-15773 Athens, Greece
[34] Physics Department, University of Oslo, Blindern, NO-1000 Oslo 3, Norway
[35] Dpto. Fisica, Univ. Oviedo, Avda. Calvo Sotelo s/n, ES-33007 Oviedo, Spain
[36] Department of Physics, University of Oxford, Keble Road, Oxford OX1 3RH, UK
[37] Dipartimento di Fisica, Università di Padova and INFN, Via Marzolo 8, IT-35131 Padua, Italy
[38] Rutherford Appleton Laboratory, Chilton, Didcot OX11 OQX, UK
[39] Dipartimento di Fisica, Università di Roma II and INFN, Tor Vergata, IT-00173 Rome, Italy
[40] Dipartimento di Fisica, Università di Roma III and INFN, Via della Vasca Navale 84, IT-00146 Rome, Italy
[41] DAPNIA/Service de Physique des Particules, CEA-Saclay, FR-91191 Gif-sur-Yvette Cedex, France
[42] Instituto de Fisica de Cantabria (CSIC-UC), Avda. los Castros s/n, ES-39006 Santander, Spain
[43] Dipartimento di Fisica, Università degli Studi di Roma La Sapienza, Piazzale Aldo Moro 2, IT-00185 Rome, Italy
[44] Inst. for High Energy Physics, Serpukov P.O. Box 35, Protvino, (Moscow Region), Russian Federation
[45] J. Stefan Institute, Jamova 39, SI-1000 Ljubljana, Slovenia and Laboratory for Astroparticle Physics,
Nova Gorica Polytechnic, Kostanjeviska 16a, SI-5000 Nova Gorica, Slovenia,
and Department of Physics, University of Ljubljana, SI-1000 Ljubljana, Slovenia
[46] Fysikum, Stockholm University, Box 6730, SE-113 85 Stockholm, Sweden
[47] Dipartimento di Fisica Sperimentale, Università di Torino and INFN, Via P. Giuria 1, IT-10125 Turin, Italy
[48] Dipartimento di Fisica, Università di Trieste and INFN, Via A. Valerio 2, IT-34127 Trieste, Italy
and Istituto di Fisica, Università di Udine, IT-33100 Udine, Italy
[49] Univ. Federal do Rio de Janeiro, C.P. 68528 Cidade Univ., Ilha do Fundão BR-21945-970 Rio de Janeiro, Brazil
[50] Department of Radiation Sciences, University of Uppsala, P.O. Box 535, SE-751 21 Uppsala, Sweden
[51] IFIC, Valencia-CSIC, and D.F.A.M.N., U. de Valencia, Avda. Dr. Moliner 50, ES-46100 Burjassot (Valencia), Spain
[52] Institut für Hochenergiephysik, Österr. Akad. d. Wissensch., Nikolsdorfergasse 18, AT-1050 Vienna, Austria
[53] Inst. Nuclear Studies and University of Warsaw, Ul. Hoza 69, PL-00681 Warsaw, Poland
[54] Fachbereich Physik, University of Wuppertal, Postfach 100 127, DE-42097 Wuppertal, Germany

1 Introduction

This paper presents a search for the production of $e^+e^- \rightarrow HZ$ with $Z \rightarrow q\bar{q}$ or $Z \rightarrow \mu^+\mu^-$ and the Higgs decaying into stable non-interacting particles rendering it invisible (see figure 1). Such invisible Higgs decays can occur in Supersymmetry[1] or other models like Majoron models [2–4] and have been previously searched for [5–7]. The search described here was performed on the data collected by DELPHI in the high energy runs of 1998 at 188.6 GeV centre-of-mass energy. The DELPHI results at energies from 161 to 183 GeV [6–8], as well as the results in the visible decay modes at 188.6 GeV [9] have been taken into account in deriving the new results.

The paper is organised as follows: first the searches with hadronic Z decays are described, followed by the search with $Z \rightarrow \mu^+\mu^-$ decays. The limits are calculated in the last section.

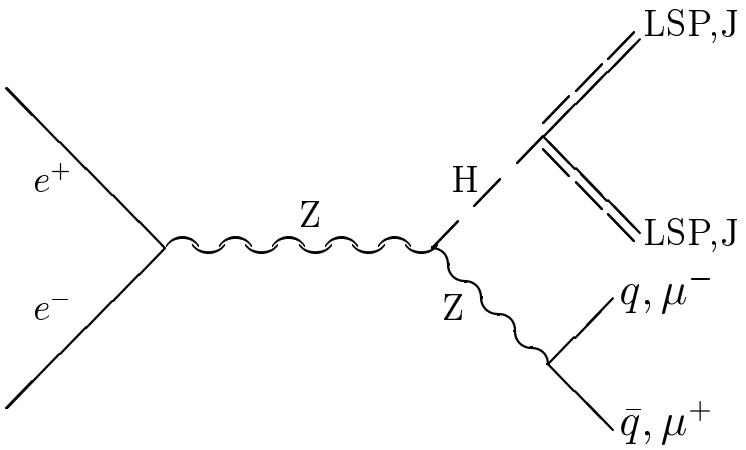

Figure 1: Feynman graph describing the HZ production with the Higgs decaying into invisible particles, e.g. the lightest supersymmetric particle (LSP) or a Majoron (J) in models with an extended Higgs sector.

2 The DELPHI Detector

The general criteria for the selection of the events are mainly based on the information from the tracking system, the calorimeters and the muon chambers of the DELPHI detector. The DELPHI detector and its performance are described in detail in [10], with the exception of the silicon tracker, which is described in [11].

3 Hadronic channel

The hadronic decay of the Z represents 69.9% of the HZ final states. The signature of an invisible Higgs boson decay is a pair of acoplanar and acollinear jets with a mass compatible with the Z mass and missing energy and momentum of the invisible decay.

The analysed data sample corresponds to an integrated luminosity of 155.3 pb^{-1} at a centre-of-mass energy of 188.6 GeV. A detector quality selection was used, requiring that

both the tracking system and the calorimeters were fully operational. The background processes $e^+e^- \to f\bar{f}(n\gamma)$ were generated using the Monte Carlo generator PYTHIA [12]. Processes leading to charged and neutral current four-fermion final states were generated with the EXCALIBUR generator [13]. In the final state $q\bar{q}e\bar{\nu}$, the GRC4F generator[14], with fermion mass effects included, was used to describe the phase space at low electron polar angles, where the finite electron mass is relevant. The TWOGAM program [15] was used to describe the two-photon interactions. For the signal simulation the HZHA Monte Carlo generator [16] was used. For this analysis samples of Higgs masses between 60 and 97.5 GeV/c^2 in 5 GeV/c^2 steps from 60 GeV/c^2 and 2.5 GeV/c^2 steps from 90 GeV/c^2 were used. Both signal and background events were processed through the full DELPHI detector simulation[10].

3.1 Event selection

Event variables were computed using reconstructed particles that satisfy the following criteria. Charged particles were defined as reconstructed tracks with momenta above 100 MeV/c, extrapolating to within 4 cm from the primary vertex in $R\phi$ and within 10 cm in z[†]. The primary vertex of the event was calculated using good quality tracks as used in beauty quark identification [17] with the additional constraint of the beam spot determined by the event vertices of nearby events. Neutral particles were defined either as calorimeter showers without associated tracks or as interaction or decay vertices in the tracking volume (e.g. converted photons and V^0 particles). The low energy thresholds depended on the particle type and the polar angle with the minimum at 100 MeV. A set of twelve variables was chosen to separate the signal from background. For most variables the event was forced in two jets or when necessary, the jets were defined with the default scaled invariant mass parameter $y_{join} = m^2_{min}/E^2_{vis} = 0.05$. The particles were clustered in jets with the LUCLUS[12] routine. These variables can be grouped together according to the different background topologies they should suppress. The first group consists of variables used to suppress the bulk of $q\bar{q}$ production, including s-channel $q\bar{q}\gamma$ production as well as t-channel two-photon interactions yielding hadrons boosted in the beam direction and little missing transverse momentum:

- E_γ/E^Z_γ : the normalised energy of a photon, assumed to have escaped in the beam direction, deduced from the polar angles of the two main jet directions in the event. The photon energy estimate was normalised to the energy expected for a photon recoiling against an on-shell Z in order to minimise the effect of small variations of the centre-of-mass energy in the data compared to simulation;
- $\not{p}_T$: the missing momentum;
- $\cos(\theta_{\mathrm{Pmis}})$: cosine of the missing momentum angle to the z-axis;
- $E(\theta < 20^\circ)/E_{vis}$: the fraction of the total visible energy below polar angles of 20°;
- Acollinearity: the acollinearity of the two jets.

A second group consists of variables used against isolated particles. In most cases these come from a W^+W^- pair decaying into $q\bar{q}'$ and a lepton or from $q\bar{q}$ production with an initial state radiated photon in the detector acceptance:

- E_{cone}/E_{isol}: the energy sum in the double cone, defined by half opening angles 5° and α_{max}, around the most isolated particle divided by its energy. The most isolated particle is defined as the particle with momentum above 2 GeV/c with the smallest

[†]The z axis is defined by the direction of the electron beam, R=$\sqrt{x^2+y^2}$ is the radius and ϕ is the azimuth angle in the xy plane.

energy sum in the double cone. In the momentum interval from 2 to 5 GeV/c, α_{max} is set to 60° in order to maximise the sensitivity to isolated particles from tau decays in $W^+W^- \to q\bar{q}'\tau\nu$ events, while an opening angle of 25° is used for particles with higher momenta;
- E_{isol}: the energy of the most isolated particle, as defined above;
- min(M_{n-jet}): the minimum jet mass in the event using the default scaled invariant mass parameter for clusterization;
- max$(p_T)_{\rm Jet}$: the highest transverse momentum of the jet-particles, defined by calculating the transverse momentum of every particle with respect to the nearest jet and taking the maximum.

The last group of variables contains information about the missing energy, momentum and mass:

- E_{vis}/E_{cms}: the total reconstructed energy, normalised to the total centre-of-mass energy;
- Acoplanarity: the log_{10} of the scaled acoplanarity. Acoplanarity is defined as 180°-$\Delta\phi$, where $\Delta\phi$ is the difference in azimuthal angle between the two jets, when forcing the reconstruction in exactly two jets. In order to compensate for the geometrical instability of this variable for jets at low polar angles it was scaled by the sine of the minimum polar angle between one of the jets and the beam axis;
- Thrust: the thrust, computed in the rest frame of the visible system. The transformation into the rest frame is made in order to compensate the smearing due to the boost of the jet system. This thrust variable defines a resolution of acoplanarity which is broader in spherical multijet events.

In addition to these variables, the visible mass M_{vis} was used in the preselection.

After a multihadronic preselection (step A) and cuts against radiative photons (step B) as described in our previous paper [7], we apply the cuts shown in table 1 (step C). The number of events remaining after each step are shown in table 2. The comparison of data and Monte Carlo simulation is satisfactory at this stage, as shown for some variables in figure 2, where any possible discrepancies are away from the regions expected for a signal. A further background reduction is obtained by an iterated nonlinear discriminant analysis (IDA), as described in [18]. The twelve variables mentioned above are used in the IDA. The number of background events after the first IDA iteration is also shown in table 2. After these cuts the signal efficiencies are around 70% for Higgs masses around 90 GeV/c^2 as shown in table 3. The background can be further reduced by a second IDA iteration at the expense of a reduction in efficiency. The residual background versus efficiency is shown in figure 3. The working point, i.e. the optimal combination of efficiency and background, determined by maximising the expected mass limit as function of efficiency, is indicated by the dashed line in figure 3.

The mass limit is determined by the Modified Frequentist Likelihood Ratio technique (MFLR) [19] using the recoil masses in the $Hq\bar{q}$ and the $H\mu^-\mu^+$ channels as input. The $Hq\bar{q}$ recoil mass, which corresponds to the mass of the invisible Higgs, is calculated from the visible energy and the visible mass using the following expression:

$$\mathrm{M}_{inv} = \sqrt{\left(E_{\rm cms} - \frac{m_{\rm Z} E_{\rm vis}}{M_{\rm vis}}\right)^2 - \left(\frac{m_{\rm Z} \not{p}}{M_{\rm vis}}\right)^2},$$

where $\not{p}$ is the missing momentum and $m_{\rm Z}$ is the Z mass.

Variable	lower cut	upper cut
E_γ/E_γ^Z	-	0.95
$\not{p}_T$	-	80 GeV/c
$E(\theta < 20°)/E_{vis}$	-	0.6
Acollinearity	-	58°
E_{isol}	-	60 GeV
$\min(M_{n-jet})$	0.5 GeV/c^2	15 GeV/c^2
E_{vis}	-	$0.65 \cdot E_{\rm cms}$
$\log_{10}$(scaled Acoplanarity)	-1.	-
Thrust	0.7	-
M_{vis}	55 GeV/c^2	100 GeV/c^2

Table 1: Hq$\bar{\rm q}$ channel: Preselection step C.

Selection	Data	total MC	q$\bar{\rm q}\nu\nu$	CC 4-f	q$\bar{\rm q}\gamma$	q$\bar{\rm q}\ell\bar{\ell}$	$\gamma\gamma$+Bhabha
Step A	17831	17115.9	26.6	2391.3	13622.7	98.3	977.0
Step B	16924	16358.5	24.0	2218.6	13109.4	94.7	911.8
Step C	1279	1177.0	21.2	132.6	888.8	6.4	128.7
1st IDA	188	177.5	19.4	74.1	80.0	0.6	3.5
final	56	65.1±1.4	15.9±0.3	33.7±1.2	15.3±0.6	0.2±0.1	0.0

Table 2: Hq$\bar{\rm q}$ channel: Data and simulated background numbers after different steps of the analysis

3.2 Results from the hadronic channel

The selected data sample consists of 56 events, with an expected background of 65.1 $\pm$ 1.4 (stat.) $^{+18.3}_{-4.0}$ (syst.) The largest background component in the final selection consists of $\rm W^+W^-$ pairs with one W boson decaying into hadrons and the other one into τ leptons with large energy escaping in neutrinos. The systematic uncertainties in the background are dominated by the imprecision of the detector simulation in reproducing tails of event variable distributions.

To study these effects, the distributions of reconstructed particle multiplicities in the simulation are smeared. The amount of particle level smearing is specified by the small deviations observed between data and simulation in a high statistics sample of hadronic

Preselection	Efficiency [%] for different m_H (GeV/c^2)									
	60	65	70	75	80	85	90	92.5	95	97.5
Step A	90.6	93.3	92.9	90.7	92.6	92.1	90.8	90.5	90.5	84.1
Step B	83.0	85.6	85.5	84.2	86.3	85.3	83.7	82.9	84.9	78.3
Step C	39.3	47.3	59.4	68.6	73.6	75.9	75.6	74.4	74.8	69.6
1st IDA	31.8	39.0	50.0	59.3	65.4	70.6	69.0	67.9	67.1	62.1
final	18.1	25.3	35.4	44.7	52.3	59.3	57.9	54.9	52.8	47.9
±(stat.)	1.2	1.4	1.5	1.6	1.6	1.5	1.4	1.5	1.6	1.6

Table 3: Hq$\bar{\rm q}$ channel: Signal efficiencies after different steps of the analysis

Z events ($\sqrt{s}$=m_Z), collected under the same experimental conditions. These smearings are applied in particle classes of different types, momenta and polar angles. Using the modified simulations and keeping the same working point, 83.1 $\pm$ 1.6(stat) events are selected. The difference was used as an asymmetric systematic error. Another source of systematics is the influence of the Monte-Carlo generator used in the analysis. The difference between the EXCALIBUR and PYTHIA four-fermion simulations contributes an error of about -5%, which is used as an asymmetric error at the lower edge, while the error obtained by the smearing dominates the high edge. The systematic uncertainties in the efficiencies were checked using a signal-like event sample of hadron jet topologies which were tagged by the presence of isolated particles (leptons from W^+W^- decays or isolated photons in $q\bar{q}\gamma$ events). The event variables were computed using the hadronic systems recoiling against the isolated particles and were passed through the selection. The agreement between the data and simulation limits the uncertainty in the signal efficiencies to a maximum of $\pm$ 10%.

4 Muon channel

The H$\mu^+\mu^-$channel represents 3.4% of the HZ final states. The experimental signature is a pair of acoplanar and acollinear muons, with an invariant mass compatible with the expectation from Z$\rightarrow\mu^+\mu^-$decays. The signal and background simulations were made with the same programs as in the hadronic channel, except that the KORALZ generator [20] was used to describe the $\mu^+\mu^-(n\gamma)$ background, the PYTHIA[12] generator was used to describe the four-fermion final states and the BHWIDE generator [21] was used for the Bhabha processes. The analysed data sample at 189 GeV corresponds to an integrated luminosity of 158.0 pb^{-1}. No data quality selection was applied.

4.1 Particle and Event selection

Charged particles were selected if their momentum was greater than 100 MeV/c and if they came from the interaction region within 10 cm along the beam direction and within 4 cm in the transverse plane. Particles with momenta more than 120% of the beam energy or with large momentum errors ($\delta p/p$ greater than 100%) were rejected. Neutral particles were selected if their associated energy in the calorimeters was above 100 MeV.

Events were required to have no more than 5 charged particles. The two fastest particles are the lepton candidates and must have opposite charges and momenta greater than 10 GeV/c. The other particles must have momenta below 5 GeV/c. This allows HZ(Z$\rightarrow\ \mu^+\mu^-$) events with two muons accompanied by an electron pair coming from the conversion of a final state radiation to be recovered. The rejection of cosmic ray events was ensured by requiring an acollinearity of the two lepton candidates greater than one degree. At least one hit in the vertex detector associated to the fastest charged particle was also required to further reduce the triggers from cosmic rays. Then the sum of the energy of all charged particles must be greater than $0.25\sqrt{s}$. At this level 96.0% of Bhabha events and 99.9% of $\gamma\gamma$ events were rejected.

A muon identification was performed for the two fastest charged particles in the event, to further reduce Bhabha and 4-fermion background. The muon identification was provided primarily by the algorithm described in [10] which relies on the association of charged particle tracks to signals in the barrel and forward muon chambers. The same algorithm has been extended to the surrounding muon chambers. The longitudinal profile of the energy deposition in the hadron calorimeter was used in addition to improve the

efficiency of the muon identification. Since 1997, the detailed information on the shape of hadronic showers as provided by the new cathode readout was used for the muon identification. The performance of the muon identification at $\sqrt{s}$ =189 GeV has been cross-checked using $Z \to \mu^+\mu^-(\gamma)$ and $Z \to \tau^+\tau^-(\gamma)$ simulated events. After the muon identification, the dominant background comes from $\mu^+\mu^-(\gamma)$ and $\gamma\gamma \to \mu^+\mu^-$ processes. No Bhabha events survive the muon identification.

Two thirds of the remaining photon-photon processes were suppressed by selecting a momentum of the faster muon greater than 43 GeV/c, and lower than 72 GeV/c. Then, the visible mass of the event must be between 76.0 GeV/c^2 and 97.5 GeV/c^2. At this level of selection, the dominant background comes from $\mu^+\mu^-\gamma$ with the photon along the beam pipe. Most of the 2-fermion and 2-photon background was suppressed after rejecting events with an acoplanarity of the muon pair with respect to the beam axis below 1.85°. The acollinearity of the muon pair must also be larger than 3.7° and below 62°. The sum of the momenta in the plane transverse to the beam axis was required to be greater than 29 GeV/c. The missing momentum had to be greater than 12.5 GeV/c and below 57.5 GeV/c, and its direction had to deviate from the beam axis by more than 22.5°.

The previous selections have been obtained by a step-wise optimisation in which each selection cut value has been varied in the search for an optimal efficiency for a given background value, iterating over the variables until a stable selection is achieved. The optimisation has been performed on half of the simulated samples and the selection was then applied to the remaining simulation samples to define unbiased efficiencies and backgrounds. Higgs boson masses from 60 to 97.5 GeV/c^2 were considered in the optimisation. The working point, i.e. the optimal combination of efficiency and background, was determined by maximising the expected limit.

4.2 Results from the muon channel

Table 4 details the effect of the selections on the data and simulated samples contributing to the background. The agreement of the data with the background simulations

selection	data	total bkg.	W^+W^-	ZZ^*	$\mu^+\mu^-(\gamma)$ $\tau^+\tau^-(\gamma)$	Ze^+e^- $We\nu_e$	$\gamma\gamma$	Bhabha	$H\mu^+\mu^-$ $\varepsilon(\%)$
Anti-cosmics	9679	9891	159	9.25	969	41.8	2039	6665	89.6
μ identification	1152	1206	35.3	4.53	648	13.7	504	0	84.6
Lepton momenta	329	335	25.8	3.17	233	7.19	65.9	0	80.3
Visible mass	121	120	6.02	1.30	106	2.55	4.02	0	71.4
Event shape	9	9.51	3.47	1.20	4.73	0.10	0	0	68.7
Miss. momentum	6	4.83	3.06	1.07	0.70	0	0	0	63.3

Table 4: $H\mu^+\mu^-$ channel: effect of the selections on data, simulated background and simulated signal events at $\sqrt{s}$ = 189 GeV. The $q\bar{q}(\gamma)$-channel is omitted in the table, because it accounts to 6.35 events after the first and 0 after the second cut. The event shape selection corresponds to the cuts on the acoplanarity, on the acollinearity and on the sum of transverse momenta. The `PYTHIA` generator was used to simulate the four-fermion processes. Efficiencies are given for a m_H=90 GeV/c^2 simulation. The zero quantities have been cross-checked by ignoring the muon identification cut with no new entries at the end.

was satisfactory after cosmic ray rejection. This can also be seen in figure 4, which shows the distributions of the acoplanarity and the acollinearity of the two lepton candidates after the cosmic ray rejection, the momentum of the faster muon and the visible mass of the event after the muon identification.

At the end of the analysis, the expected background comes mainly from W^+W^-, and amounts to 4.83 $\pm$ 0.64 (stat) $\pm$ 0.46 (syst) events. The systematics were derived as explained in [7]. In order to check the sensitivity to generator level effects, the four-fermion processes obtained with `PYTHIA` and `EXCALIBUR` were compared at each step of the selection, as shown in table 5.

The signal efficiencies for different Higgs boson masses are given in Table 6. After the combination with the results obtained in the $H\mu^+\mu^-$ channel at $\sqrt{s}$ = 183 GeV [7], 8 events are left in the data, compared to 6.57 ± 0.69 (stat) ± 0.75 (syst) expected from the simulation.

Selection $\sqrt{s}$=189 GeV	Data	bkg. PYTHIA 4-f	bkg. EXCALIBUR 4-f
Anti-cosmics	9 679	$9\,891 \pm 155$	$9\,874 \pm 155$
μ identification	1 152	$1\,206 \pm 21$	$1\,192 \pm 21$
Lepton momenta	329	335 ± 9	327 ± 9
Visible mass	121	120 ± 4	118 ± 4
Event shape	9	9.51 ± 0.96	9.71 ± 0.87
Miss. momentum	6	4.83 ± 0.64	5.29 ± 0.53

Table 5: $H\mu^+\mu^-$ channel – The expected backgrounds are compared when PYTHIA or EXCALIBUR is used as 4-fermion generator.

m_H (GeV/c^2)	Efficiency (%)
60.0	$37.5 \pm 1.1\ ^{+0.8}_{-1.2}$
65.0	$47.8 \pm 1.1\ ^{+1.3}_{-0.9}$
70.0	$53.8 \pm 1.1\ ^{+1.2}_{-1.5}$
75.0	$58.4 \pm 1.1\ ^{+1.6}_{-1.1}$
80.0	$61.0 \pm 1.1\ ^{+1.3}_{-1.4}$
85.0	$63.4 \pm 1.1\ ^{+1.7}_{-1.3}$
90.0	$63.3 \pm 1.1\ ^{+1.2}_{-1.2}$
92.5	$61.9 \pm 1.1\ ^{+1.4}_{-1.5}$
95.0	$46.3 \pm 1.1\ ^{+1.9}_{-1.8}$
97.5	$34.9 \pm 1.0\ ^{+2.5}_{-2.3}$

Table 6: $H\mu^+\mu^-$ channel: efficiency of the selection at $\sqrt{s}$ = 189 GeV as a function of the mass of the Higgs boson. The first errors given are statistical, the second ones are systematic.

5 Limits

5.1 Model independent limits

In this letter, we define model-independent by being independent of the relative branching ratios between visible SM and invisible Higgs boson decays, while a SM production cross section is assumed.

The cross-section and mass limits were computed again with the MFLR method [19]. The event rates in the analysis of the DELPHI $\sqrt{s}$ = 161 to 172 GeV data[6], and the distributions of the reconstructed masses at 183 GeV [7] and 189 GeV were included in the likelihood function. The distribution of reconstructed missing masses of muon pair and hadronic candidates at 183 GeV and 189 GeV is shown in figure 5.

Figure 6 displays the observed and expected upper limits on the cross-section for the process $e^+e^- \to Z(\text{anything})H(\text{invisible})$ as a function of the Higgs mass. From the comparison with the Standard Model Higgs cross-section the observed (expected) mass limits are 93.8 (89.7) GeV/c^2.

In general, the branching ratio into invisible particles BR_{inv} can be a free parameter and the remaining decay modes are then visible and are assumed to follow the SM decay probabilities. In this case the searches for visible and invisible Higgs decays can be combined to determine the excluded region in the BR versus m_H plane assuming SM production cross-sections. Using the DELPHI limits on the visible cross-section [9] a lower mass limit of 92.3 GeV/c^2 can be set independent of the hypothesis on the fraction of invisible decay modes, as shown in figure 7. In computing these limits, the overlap between the standard $H\nu\bar{\nu}$ and the invisible Higgs hadronic selections have been resolved, conservatively for the limit, by omitting the $H\nu\bar{\nu}$ ($H_{inv}q\bar{q}$) results in the region $BR_{inv} > 50\% (< 50\%)$.

5.2 Limits for a Majoron Model

The limits computed above can be used to set a limit on the Higgs bosons in a Majoron model with one doublet ϕ and one singlet η. Mixing of the real parts of ϕ and η leads to two massive Higgs bosons:

$$H = \phi_R \cos\theta - \eta_R \sin\theta$$

$$S = \phi_R \sin\theta + \eta_R \cos\theta$$

where θ is the mixing angle. The imaginary part of the singlet is identified as the Majoron. The Majoron is decoupled from the fermions and gauge bosons, but might have a large coupling to the Higgs bosons. In this model the free parameters are the masses of H and S, the mixing angle θ and the ratio of the vacuum expectation values of the two fields ϕ and η ($\tan\beta \equiv \frac{v_\phi}{v_\eta}$). The production rates of the H and S are reduced with respect to the SM Higgs boson, by factors of $\cos^2\theta$ and $\sin^2\theta$, respectively. The decay widths of the H and S into the heaviest possible fermion-antifermion pair are reduced by the same factor and their decay widths into a Majoron pair are proportional to the complementary factors ($\cos^2\theta$ for S and $\sin^2\theta$ for H). Concentrating on the case where the invisible Higgs decay mode is dominant ($\tan\beta$ large), the excluded region in the mixing angle versus Higgs mass plane is shown in figure 8.

6 Conclusion

In data samples of 155.3 pb^{-1} for the $q\bar{q}$ channel and 158 pb^{-1} for $\mu^+\mu^-$ channel collected by the DELPHI detector at a centre-of-mass energy of 189 GeV, 56 hadronic events and 6 muon pair events were selected with expected backgrounds of $65.1^{+18.3}_{-4.2}$ and 4.8 ± 0.8, respectively.

Combining these results and the earlier DELPHI analyses, we set a 95% CL lower mass limit of 93.8 GeV/c^2 for Higgs bosons with a Standard Model cross-section and with 100% branching fraction into invisible decays. By combining this search for invisible decays with previous limits on visible decays we can set a 95% CL lower mass limit of 92.3 GeV/c^2 for a Higgs boson with an arbitrary invisible branching fraction.

Acknowledgements

We are greatly indebted to our technical collaborators, to the members of the CERN-SL Division for the excellent performance of the LEP collider, and to the funding agencies for their support in building and operating the DELPHI detector.
We acknowledge in particular the support of
Austrian Federal Ministry of Science and Traffics, GZ 616.364/2-III/2a/98,
FNRS–FWO, Belgium,
FINEP, CNPq, CAPES, FUJB and FAPERJ, Brazil,
Czech Ministry of Industry and Trade, GA CR 202/96/0450 and GA AVCR A1010521,
Danish Natural Research Council,
Commission of the European Communities (DG XII),
Direction des Sciences de la Matière, CEA, France,
Bundesministerium für Bildung, Wissenschaft, Forschung und Technologie, Germany,
General Secretariat for Research and Technology, Greece,
National Science Foundation (NWO) and Foundation for Research on Matter (FOM), The Netherlands,
Norwegian Research Council,
State Committee for Scientific Research, Poland, 2P03B06015, 2P03B1116 and SPUB/P03/178/98,
JNICT–Junta Nacional de Investigação Científica e Tecnológica, Portugal,
Vedecka grantova agentura MS SR, Slovakia, Nr. 95/5195/134,
Ministry of Science and Technology of the Republic of Slovenia,
CICYT, Spain, AEN96–1661 and AEN96-1681,
The Swedish Natural Science Research Council,
Particle Physics and Astronomy Research Council, UK,
Department of Energy, USA, DE–FG02–94ER40817.

References

[1] A. Djouadi, P. Janot, J. Kalinowski and P.M. Zerwas, *Phys. Lett.* **B376** (1996) 220

[2] Y. Chikashige, R.N. Mohapatra, R.D. Peccei, *Phys. Lett.* **B98** (1981) 265;
R.E. Shrock, M. Suzuki, *Phys. Lett.* **B110** (1982) 250;
R. Mohapatra, J.W.F. Valle, *Phys. Rev.* **D34** (1986) 1642;
M.C. Gonzalez-Garcia, J.W.F. Valle, *Phys. Lett.* **B216** (1989) 360;
E.D Carlson, L.J. Hall, *Phys. Rev.* **D40** (1989) 3187;
L.F. Li,Y. Liu, L. Wolfenstein, *Phys. Lett.* **B159** (1985) 45;
A. Zee, *Phys. Lett.* **B93** (1980) 389.

[3] F. de Campos et al.,*Phys. Rev.* **D55** (1997) 1316.

[4] S.P. Martin and J.D. Wells, *Phys. Rev.* **D60** (1999) 035006

[5] ALEPH Collaboration, R. Barate et al., *Phys. Lett.* **B450** (1999) 301 and *Phys. Lett.* **B466** (1999) 50
L3 Collaboration, M.Acciarri et al., *Phys. Lett.* **B385** (1996) 454 and *Phys. Lett.* **B418** (1998) 389
L3 Collaboration, M.Acciarri et al., *Search for an invisibly decaying Higgs boson in e^+e^- collisions at $\sqrt{s}$ = 183-189 GeV* CERN-EP-2000-047
OPAL Collaboration, G.Alexander et al., *Phys. Lett.* **B377** (1996) 273

[6] DELPHI Collaboration, P. Abreu et al., *Eur. Phys. J.* **C2** (1998) 1.

[7] DELPHI Collaboration, P. Abreu et al., *Phys. Lett.* **B459** (1999) 367

[8] DELPHI Collaboration, P. Abreu et al., *Eur. Phys. J.* **C10** (1999) 563.

[9] DELPHI Collaboration, P. Abreu et al., *Search for neutral Higgs bosons in e^+e^- collisions at $\sqrt{s}$=188.7 GeV*,CERN-EP-2000-038 accepted by *Eur. Phys. J.* **C**

[10] DELPHI Collaboration, P. Abreu et al., *Nucl. Instr. and Meth.* **A378** (1996) 57 DELPHI Collaboration, P. Aarnio et al, *Nucl. Instr. and Meth.* **A303** (1991) 233

[11] DELPHI Silicon Tracker Group,P. Chochula et al., *Nucl. Instr. and Meth.* **A412** (1998) 304

[12] T. Sjöstrand, *Comp. Phys. Comm.* **39** (1986) 347; *Comp. Phys. Comm.* **82** (1994) 74.

[13] F.A. Berends, R. Pittau, R. Kleiss, *Comp. Phys. Comm.* **85** (1995) 437.

[14] Y. Kurihara et al., Vol. 2, p. 30 in *Physics at LEP2* G. Altarelli, T. Sjöstrand and F. Zwirner (eds.) CERN 96-01 (1996).

[15] S. Nova et al. in CERN Report 96-01, Vol. 2, p. 224.

[16] P. Janot, in CERN Report 96-01, Vol. 2, p. 309.

[17] DELPHI Collaboration, P. Abreu et al., *Eur. Phys. J.* **C10** (1999) 415.

[18] T.G.M. Malmgren, *Comp. Phys. Comm.* **106** (1997) 230;
T.G.M. Malmgren and K.E. Johansson, *Nucl. Instr. and Meth.* **A403** (1998) 481.

[19] A.L. Read, *Optimal statistical analysis of search results based on the likelihood ratio and its application to the search for the MSM Higgs boson at $\sqrt{s}$ = 161 and 172 GeV,* DELPHI 97-158 PHYS 737.

[20] S. Jadach, B. F. Ward and Z. Was, *Comp. Phys. Comm.* **79** (1994) 503.

[21] S. Jadach, W. Placzek and B. F. Ward, *Phys. Lett.* **B390** (1997) 298

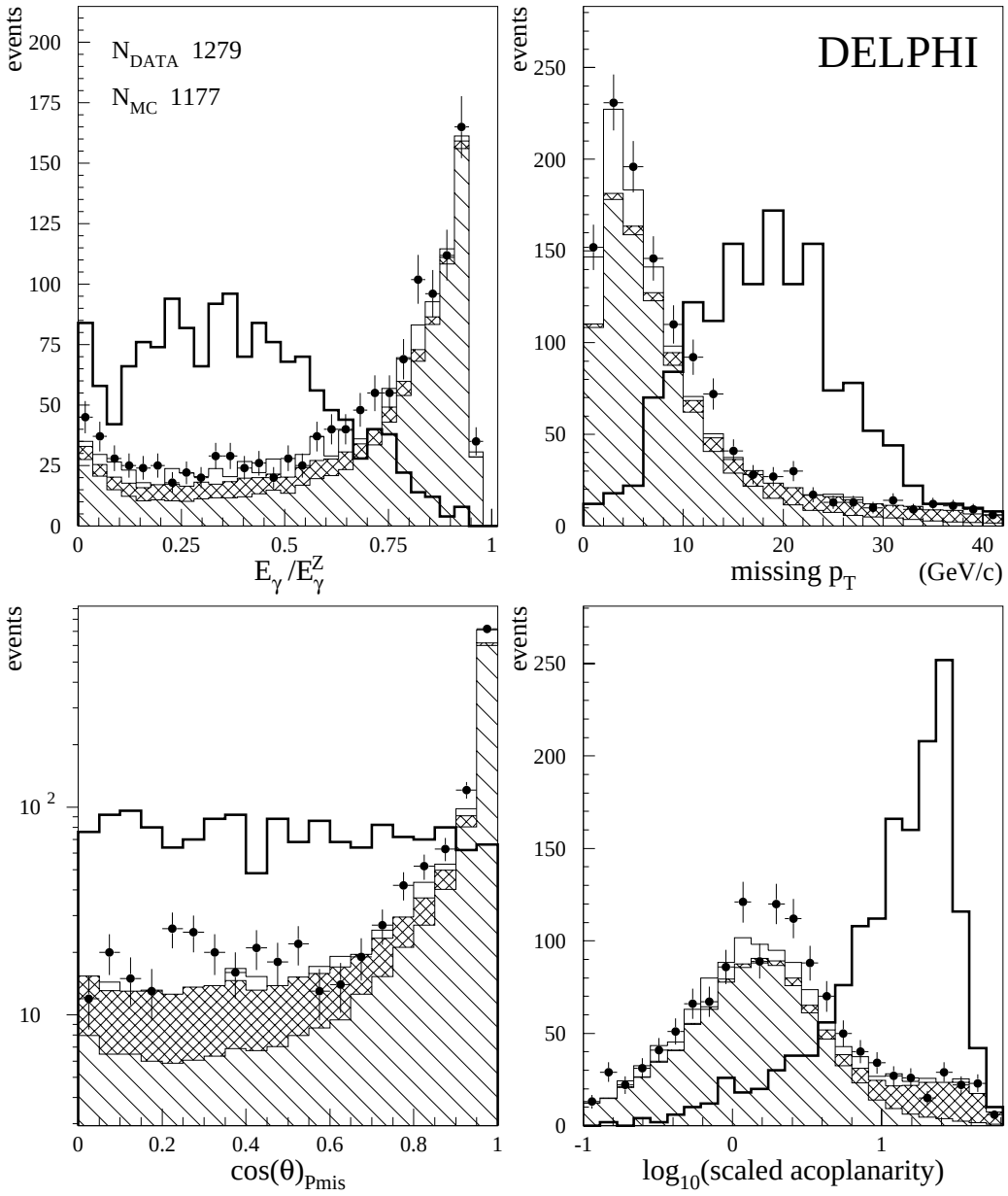

Figure 2: Hq$\bar{\text{q}}$ channel – a comparison of data (dots) and simulated background for various variables of the Hq$\bar{\text{q}}$ channel after the selection step C. The upper histogram line (thin) is the sum of qq(γ) (hatched), 4-fermion background (double hatched), $\gamma\gamma$ and a small contribution from Bhabha processes(white). The thick line is the expected signal distribution for a 90 GeV/c^2 Higgs boson scaled by a factor of 2000.

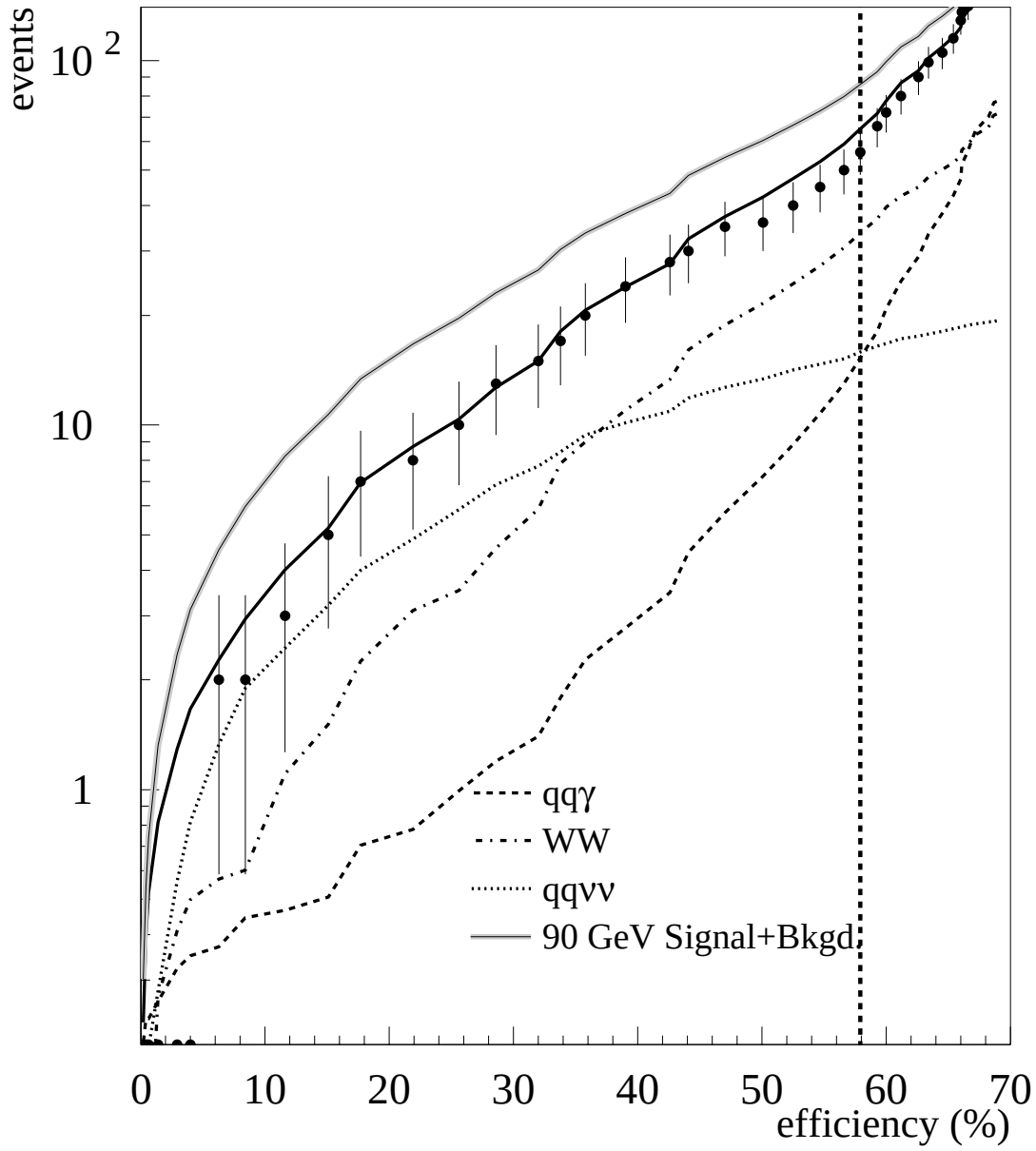

Figure 3: Hq$\bar{\text{q}}$ channel – The expected background as function of the efficiency for a Higgs signal of 90 GeV/c^2. The indicated lines represent the most important backgrounds with the black line showing the sum of all the backgrounds. The vertical dashed line marks the working point, which has been calculated for a Higgs mass of 85 GeV/c^2.

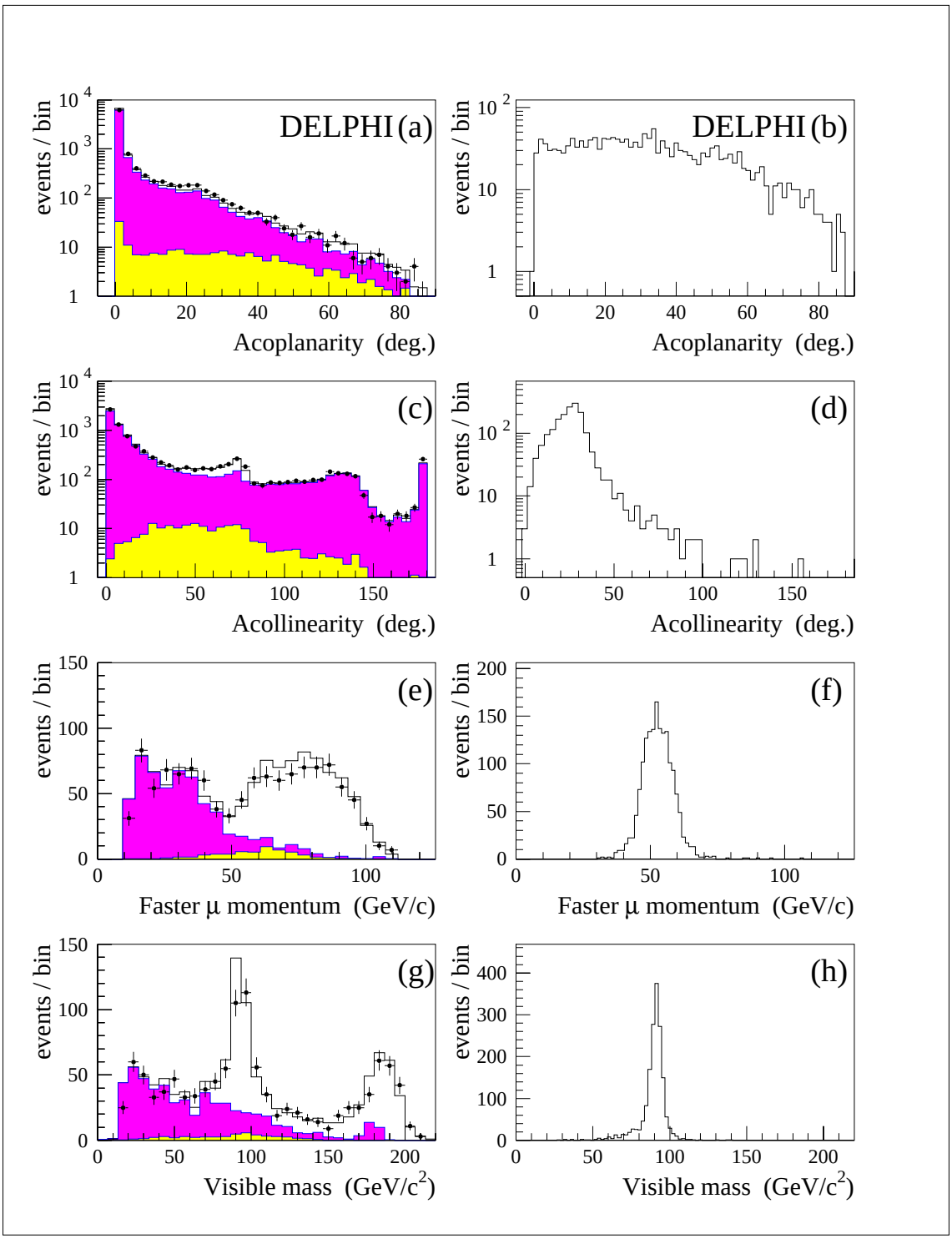

Figure 4: H$\mu^+\mu^-$ analysis: distributions of the acoplanarity (a-b) and of the acollinearity (c-d) of the two muon candidates after the rejection of cosmic ray events; distributions of the momentum of the faster muon (e-f) and of the visible mass (g-h) after the muon identification. Plots on the left show a comparison between $\sqrt{s}$ =189 GeV data (points) and simulated background events (solid line) normalised to the experimental luminosity. The light grey area represents the contribution from the 4-fermion background, the dark grey the contribution of Bhabha and 2-photon processes, and the white area the contribution of ll(γ). Plots on the right show the unnormalised expected distributions for a Higgs boson of 90 GeV/c^2.

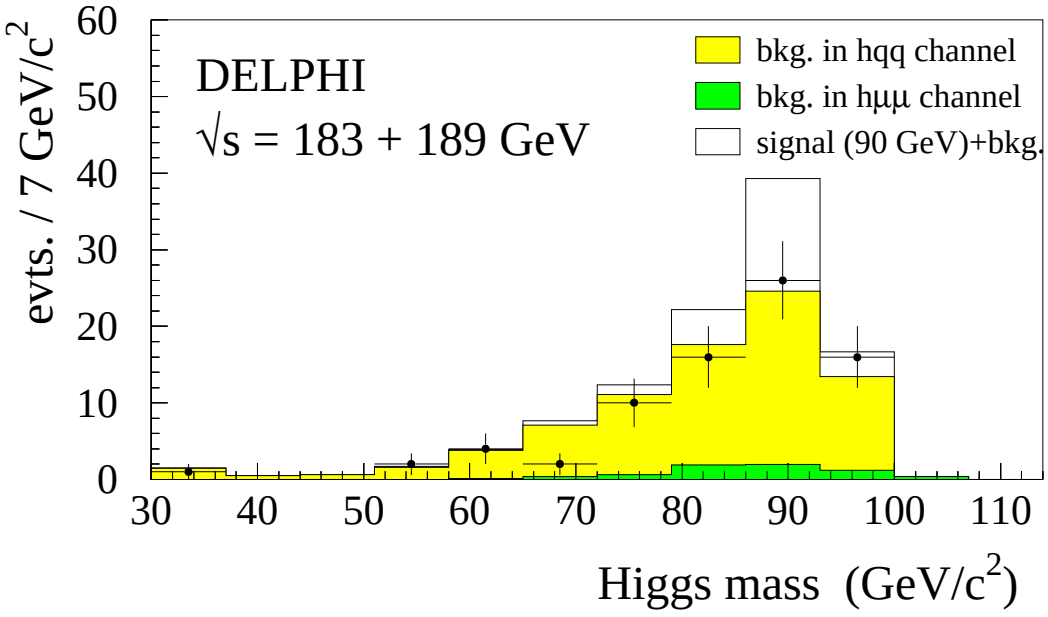

Figure 5: Distribution of missing masses of $Hq\bar{q}$ and $H\mu^+\mu^-$ event candidates at 183 and 189 GeV.

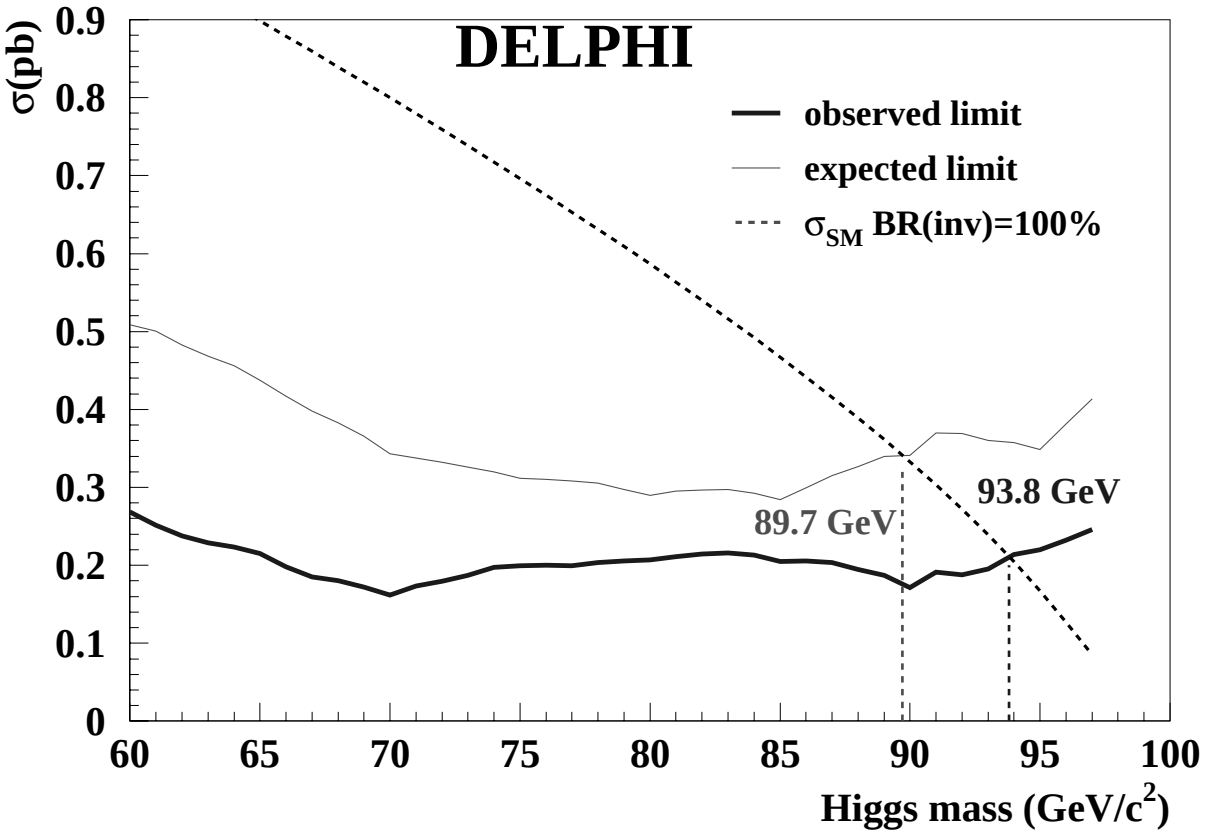

Figure 6: The 95% CL upper limit on the cross-section $e^+e^- \to Z(\text{anything})\,H(\text{invisible})$ as a function of the Higgs boson mass. The dashed line shows the standard model cross-section for the Higgs production with a BR_{inv} of 100%.

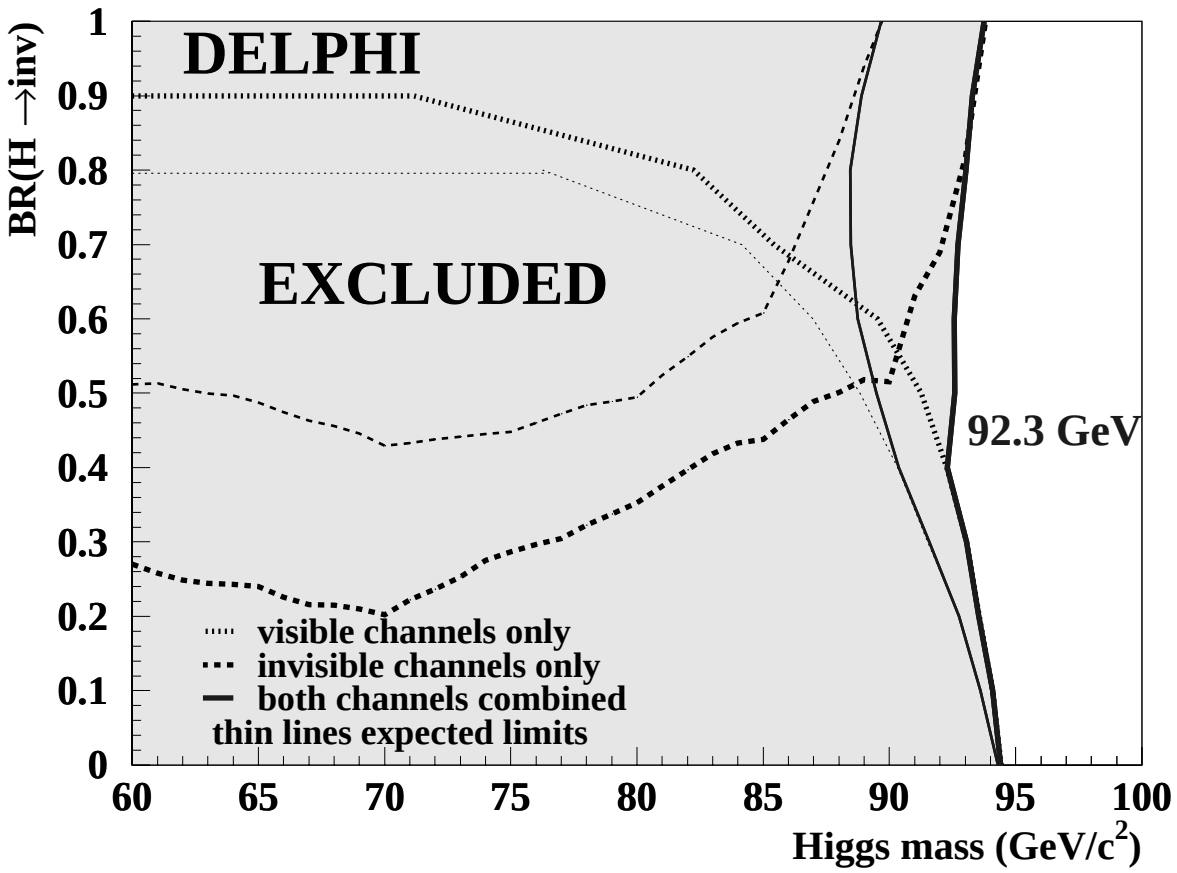

Figure 7: The excluded Higgs limits as function of the branching ratio into invisible decays BR_{inv}, assuming a $1 - BR_{inv}$ branching ratio into standard visible decay modes.

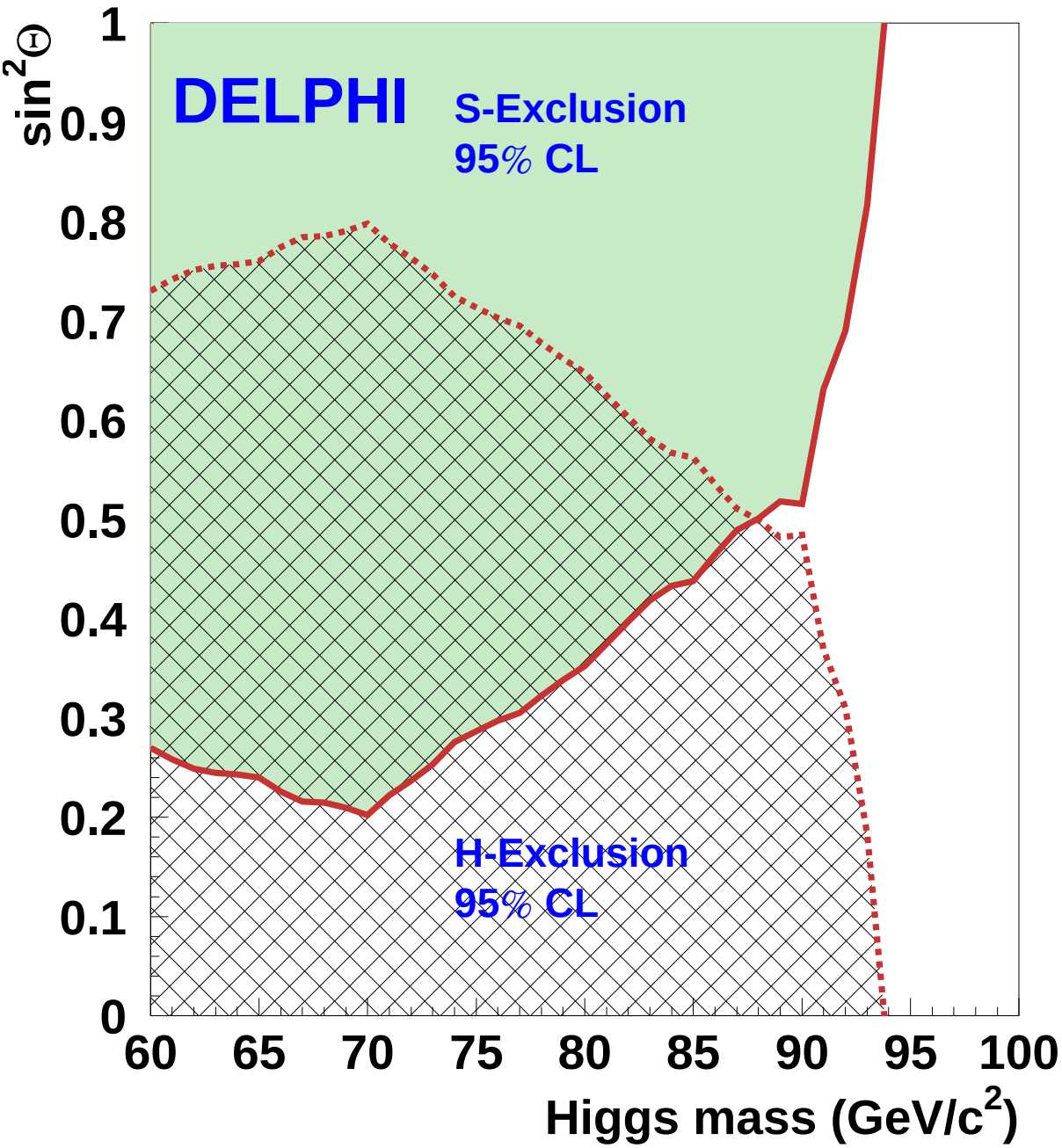

Figure 8: Limit on $\sin^2\theta$ as a function of the Higgs mass at 95% CL. S and H are the Higgs bosons in the Majoron model with expected production rates for large $\tan\beta$. In this case the Higgs boson only decays invisibly.